

## Activation of ectopic olfactory receptor 544 induces GLP-1 secretion and regulates gut inflammation

Chunyan Wu<sup>a†</sup>, Mi-Young Jeong<sup>a†</sup>, Jung Yeon Kim<sup>a</sup>, Giljae Lee<sup>b,c</sup>, Ji-Sun Kim<sup>a</sup>, Yu Eun Cheong<sup>a</sup>, Hyena Kang<sup>b,c</sup>, Chung Hwan Cho<sup>b,c</sup>, Jimin Kim<sup>a</sup>, Min Kyung Park<sup>d</sup>, You Kyoung Shin<sup>e</sup>, Kyoung Heon Kim<sup>a</sup>, Geun Hee Seol<sup>e</sup>, Seung Hoi Koo<sup>f</sup>, GwangPyo Ko<sup>b,c</sup>, and Sung-Joon Lee<sup>g</sup> 

<sup>a</sup>Department of Biotechnology, School of Life Science and Biotechnology for BK21 Plus, Korea University, Seoul, Republic of Korea;

<sup>b</sup>Department of Environmental Health Sciences, Seoul National University, Seoul, Republic of Korea; <sup>c</sup>Center for Human and Environmental Microbiome, Seoul National University, Seoul, Republic of Korea; <sup>d</sup>Department of Food Science and Engineering, Ewha Womans University, Seoul, Republic of Korea; <sup>e</sup>Department of Basic Nursing Science, School of Nursing, Korea University, Seoul, Republic of Korea; <sup>f</sup>Division of Biological Sciences, College of Life Sciences and Biotechnology, Korea University, Seoul, Republic of Korea; <sup>g</sup>Department of Food Bioscience and Technology, College of Life Sciences and Biotechnology, Korea University, Seoul, Republic of Korea

### ABSTRACT

Olfactory receptors are ectopically expressed in extra-nasal tissues. The gut is constantly exposed to high levels of odorants where ectopic olfactory receptors may play critical roles. Activation of ectopic olfactory receptor 544 (Olfr544) by azelaic acid (AzA), an Olfr544 ligand, reduces adiposity in mice fed a high-fat diet (HFD) by regulating fuel preference to fats. Herein, we investigated the novel function of Olfr544 in the gut. In GLUTag cells, AzA induces the cAMP-PKA-CREB signaling axis and increases the secretion of GLP-1, an enteroendocrine hormone with anti-obesity effects. In wild-type (WT) mice injected AzA, GLP-1 plasma levels were elevated. The induction of GLP-1 secretion was negated in cells with Olfr544 gene knockdown and in Olfr544-deficient mice. Gut microbiome analysis revealed that AzA increased the levels of *Bacteroides acidifaciens* and microbiota associated with antioxidant pathways. In fecal metabolomics analysis, the levels of succinate and trehalose, metabolites correlated with a lean phenotype, were elevated by AzA. The function of Olfr544 in gut inflammation, a key feature in obesity, was further investigated. In RNA sequencing analysis, AzA suppressed LPS-induced activation of inflammatory pathways and reduced TNF- $\alpha$  and IL-6 expression, thereby improving intestinal permeability. The effects of AzA on the gut metabolome, microbiome, and colon inflammation were abrogated in Olfr544-KO mice. These results collectively demonstrated that activation of Olfr544 by AzA in the gut exerts multiple effects by regulating GLP-1 secretion, gut microbiome and metabolites, and colonic inflammation in anti-obesogenic phenotypes and, thus, may be applied for obesity therapeutics.

### ARTICLE HISTORY

Received 26 May 2021  
Revised 31 August 2021  
Accepted 16 September 2021

### KEYWORDS

Olfr544; ectopic olfactory receptor; GLP-1; gut microbiome; metabolome; colonic inflammation

## Introduction


Olfaction is the most sensitive sensory system in mammals that has evolved to optimize survival in nature.<sup>1</sup> Olfactory receptors (ORs), which are primarily expressed in the cilia of olfactory sensory neurons, recognize odorants as ligands and stimulate signal transduction pathways to transfer odorant information to the brain.<sup>2</sup> ORs are classic G protein-coupled receptors, which constitute approximately 5–10% of the mammalian genome. The results of RNA-Seq analysis demonstrated that ORs are also ectopically expressed in extra-nasal tissues.<sup>3</sup> Ectopic ORs play tissue-specific functions,

including the regulation of sperm chemotaxis, adiposity, lipid metabolism, wound healing, hair growth, muscle regeneration, and cancer cell growth.<sup>4</sup> These findings suggest that extra-nasal tissues can also sense odors in an OR-dependent manner to regulate several cellular activities.

Olfr544, a mouse OR, is widely expressed in diverse tissues, including the small intestine, colon, adipose tissue, liver, and skeletal muscle. Activation of Olfr544 by its ligand, azelaic acid (AzA), was reported to show anti-obesogenic effects in high-fat diet (HFD)-fed mice by regulating inter-organ energy metabolism, including the induction of lipolysis in white adipose

**CONTACT** Sung-Joon Lee  [junelee@korea.ac.kr](mailto:junelee@korea.ac.kr)  Department of Biotechnology, School of Life Science and Biotechnology for BK21 Plus, Korea University, Seoul, Republic of Korea

<sup>†</sup>These authors contributed equally to this work.

 Supplemental data for this article can be accessed on the [publisher's website](#).

© 2021 The Author(s). Published with license by Taylor & Francis Group, LLC.

This is an Open Access article distributed under the terms of the Creative Commons Attribution-NonCommercial License (<http://creativecommons.org/licenses/by-nc/4.0/>), which permits unrestricted non-commercial use, distribution, and reproduction in any medium, provided the original work is properly cited.

tissue (WAT), thermogenesis in brown adipose tissue (BAT), and fatty acid oxidation in the liver.<sup>5</sup> Activation of Olfr544 increases mitochondrial biogenesis in skeletal myotubes by a protein kinase A (PKA)-dependent mechanism;<sup>6</sup> this activation also induces the secretion of glucagon in pancreatic  $\alpha$ -cells.<sup>7</sup> AzA is a nine-carbon saturated dicarboxylic acid that is commonly found in wheat, barley, and rye; it is endogenously synthesized by hepatic  $\omega$ -oxidation of medium-chain fatty acids.<sup>8</sup>

AzA has several biological activities. The administration of AzA has been reported to exhibit an anti-atherogenic effect in mice, reduce atherosclerotic lesion size, and suppress pro-inflammatory cytokine gene expression in the aorta.<sup>9</sup> The administration of AzA was found to ameliorate lipid and glucose metabolism in mice,<sup>10</sup> consistent with the results of our previous report.<sup>5</sup> AzA is known for its anti-inflammatory, anti-bacterial, anti-keratinizing, and anti-tumor activities.<sup>11–13</sup> These effects are also presumed to be dependent on activation of Olfr544, but this hypothesis has not yet been investigated. Ectopic ORs may play important functions, especially in tissues that are consistently exposed to high concentrations of diverse odorants. In this context, there is a need to examine the role of ectopic ORs in the gut, because of the continuous exposure to large amounts of exogenous and endogenous odorants in the gut. In this study, we investigated the mechanism of action of Olfr544 in the gut, with respect to regulation of adiposity and inflammation. Activation of Olfr544 induced glucagon-like peptide-1 (GLP-1), an enteroendocrine hormone secreted by L cells, through a PKA-dependent mechanism. Activation of Olfr544 also modulated the fecal metabolome and gut microbiota, thus resulted in anti-inflammatory effects.

## Results

### ***Olfr544 is functionally expressed in mouse small intestine and colon tissues and GLUTag cells***

Olfr544 is widely expressed in several extra-nasal tissues; activation by its ligand, AzA, shifts fuel preference to fats and reduces adiposity.<sup>5</sup> Thus, Olfr544 expression in the gut was examined in this study. RT-PCR and qPCR

analyses indicated that *Olfr544* was expressed in the mouse small intestine (ileum, jejunum and duodenum) and colon tissues (Figure 1(a)) as well as in GLUTag cells, a mouse intestinal L cell line (Figure 1(b)). *Chromogranin A* (*Chg*), a general marker of enteroendocrine cells and *glucagon* (*Gcg*) were also expressed in the GLUTag cells (Figure 1(b)). Olfr545, which is homologous to Olfr544, was found to be expressed in mouse small intestine and colon tissues, but at markedly lower levels than Olfr544 (Figure 1(a)). Considering the low expression level of Olfr545 and its lower binding affinity to AzA compared to Olfr544 ( $EC_{50}$  of AzA 29.7 and 537.4  $\mu$ M for Olfr544 and Olfr545, respectively).<sup>5</sup> Olfr544 is the major receptor for AzA in the gut; Olfr545 is not. The role of the activation of Olfr545 by AzA in the gut may be negligible.

### ***Olfr544 activation by AzA induces GLP-1 secretion in mice***

Gut hormones are known to play key roles in controlling whole-body energy metabolism and inflammation.<sup>14</sup> Therefore, we investigated whether Olfr544 activation regulates enteroendocrine hormone levels. Acute injection of AzA did not affect the plasma hormone levels of peptide YY (PYY), GLP-2, gastric inhibitory polypeptide (GIP) or ghrelin in wild-type (WT) mice (Supplementary Figure 1). However, treatment of AzA *ex vivo* and acute injection of AzA *in vivo* induced GLP-1 secretion in WT mice (Figure 1(c)). The induction of GLP-1 secretion by AzA was negated in Olfr544-KO mice, both in *ex vivo* and *in vivo* (Figure 1(c)). Immunoblotting analysis showed that the level of cyclic AMP-responsive element-binding protein (CREB) phosphorylation was induced 30 and 120 minutes after intraperitoneal injection of AzA in mouse small intestine tissues (Figure 1(d)). In mice fed an AzA-containing HFD for 6 weeks, AzA intake reduced body weight and adiposity (Supplementary Figure 2a) in WT mice without affecting food intake (data not shown), plasma lipids, and GLP-1 levels in fasting state (Supplementary

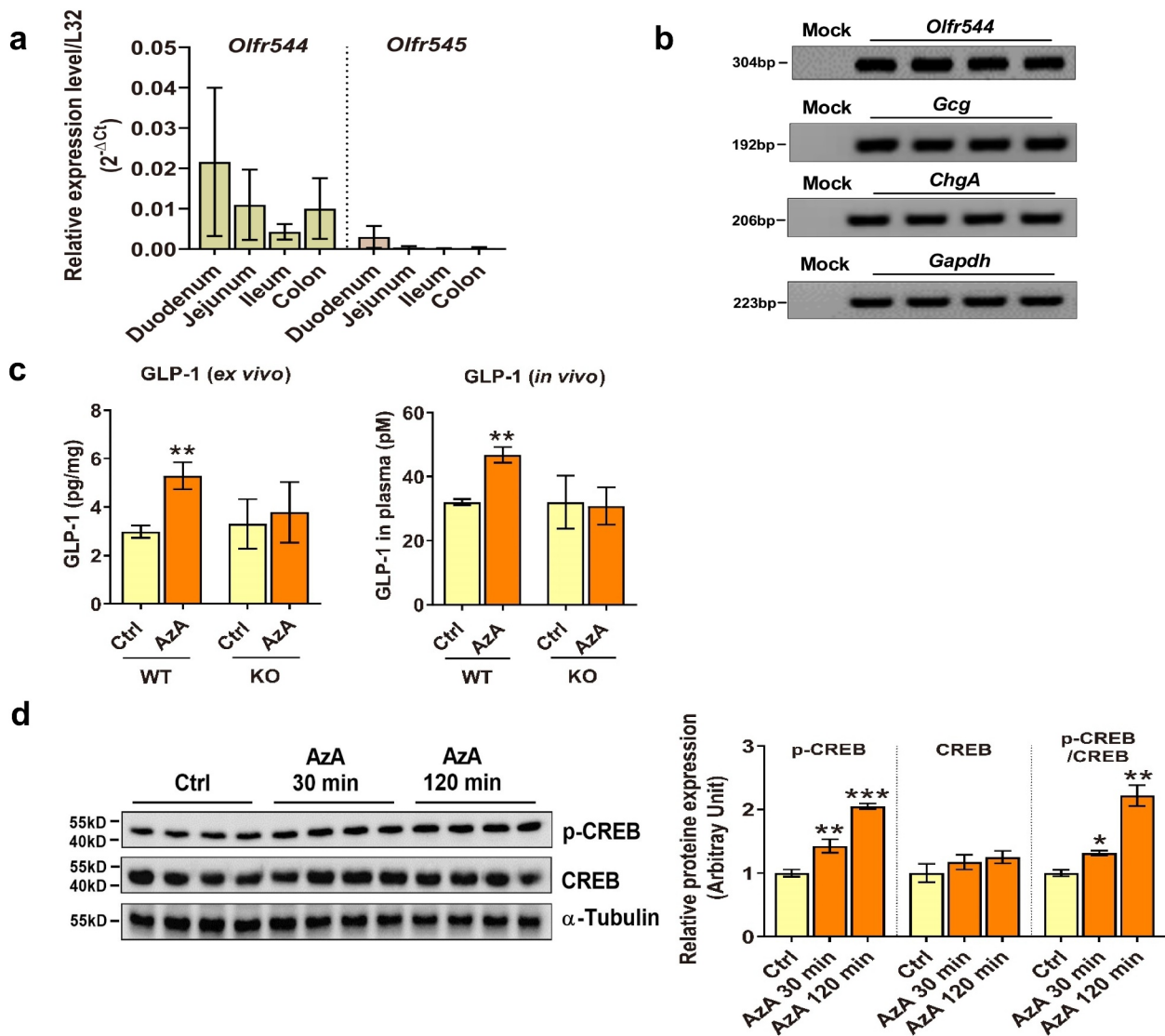


**Figure 1.** *Olf544* activation induces GLP-1 secretion via CREB phosphorylation in mice small intestine. (a) *Olf544* and *Olf545* expression by qPCR in mouse small intestine and colon tissues. (b) *Olf544*, *Gcg*, and *ChgA* expression by RT-PCR in GLUTag cells. (c) Acute AzA injection induced GLP-1 secretion in mice in both *ex vivo* and *in vivo* conditions in wild-type C57BL/6 J mice ( $n = 4-5$ ) but not in *Olf544*-knockout mice ( $n = 5-8$ ). (d) Immunoblot analysis of CREB and phosphorylated CREB (p-CREB) ( $n = 3$ ). Ctrl, control; AzA, azelaic acid (50  $\mu$ M). The data are presented as the mean  $\pm$  SEM. One-way ANOVA followed by Tukey's HSD test and Student t-test were performed for multiple- and two group comparisons. Different asterisks indicate a significant difference at \* $P < .05$ , \*\*  $P < .01$ , \*\*\*  $P < .01$  compared with controls.

Figure 2b). Hepatic triglyceride concentrations and liver enzyme levels, especially alanine transaminase (ALT) levels, were significantly reduced (Supplementary Figure 2c). Thyroid hormone levels were not enhanced by AzA (Supplementary Figure 2d). These results demonstrated that *Olf544* activation by AzA induces CREB activity and GLP-1 secretion in the mouse small intestine.

### ***Olf544* activation induces GLP-1 secretion in GLUTag cells**

We next investigated the mechanism of GLP-1 secretion by AzA in GLUTag cells. Activation of *Olf544* by AzA (50  $\mu$ M) significantly induced GLP-1 secretion (Figure 2(a)), but not other hormone secretion such as GLP-1 and PYY (data not shown), cell viability, proliferation, mitochondrial

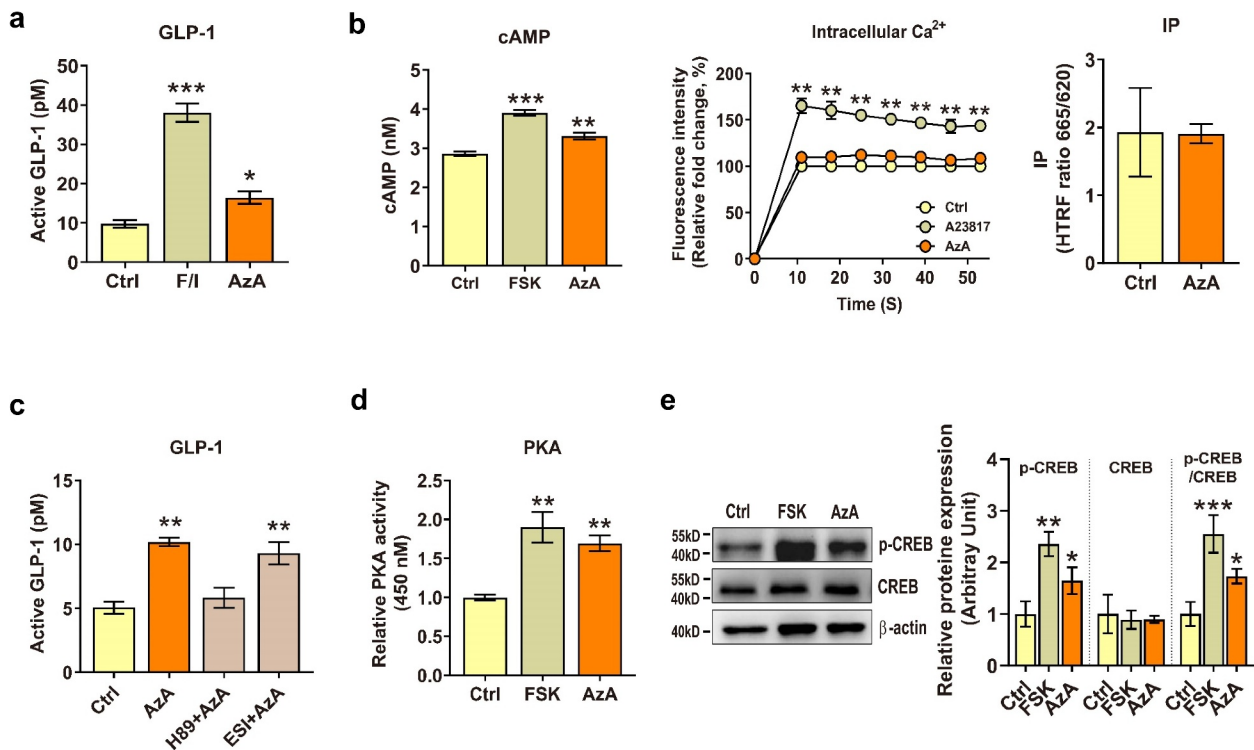


**Figure 2.** Activation of Olfr544 by AzA activates the cAMP-PKA signaling axis and induces GLP-1 secretion in GLUTag cells. (a) Olfr544 activation by AzA induces GLP-1 secretion ( $n = 6$ ). (b) AzA increases cAMP concentrations ( $n = 5$ ), but not intracellular calcium ( $n = 9$ ) or inositol phosphate (IP) levels ( $n = 5$ ). HTRF ratio, homogeneous time-resolved fluorescence ratio (665 nm/620 nm). (c) GLP-1 secretion by GLUTag cells incubated with a PKA inhibitor (H89) or an EPAC inhibitor (ESI-09) ( $n = 3$ ). (d) Relative PKA activity ( $n = 4$ ), and (e) immunoblot analysis of CREB and phosphorylated CREB (p-CREB) ( $n = 3$ ). Ctrl, control; F/I, 10  $\mu$ M forskolin and 10  $\mu$ M IBMX; FSK, forskolin (10  $\mu$ M); AzA, azelaic acid (50  $\mu$ M); A-23187 (10  $\mu$ M), a calcium-ionophore positive control. The data are presented as the mean  $\pm$  SEM. One-way ANOVA with Bonferroni's test and Student t-test were performed for multiple- and two group comparisons. \* $P < .05$ , \*\* $P < .01$ , \*\*\* $P < .001$  compared with controls.

biogenesis, and apoptosis in GLUTag cells (Supplementary Figure 3(a) and (b)). Gut hormones could play important roles in the regulation of blood pressure thus, we examined the effects of AzA on blood pressure in rats. Results showed that oral administration of AzA for 5 days did not affect heart rate and blood pressure in rats (data not shown). Signal transduction pathways mediating GLP-1 secretion were investigated. Quantification of second messengers revealed that AzA upregulated cAMP concentration but did not alter intracellular calcium or inositol phosphate levels (Figure 2(b)). Induction of cAMP by AzA could activate either PKA or exchange proteins activated by cAMP (EPAC).<sup>15,16</sup> Next, cells stimulated with AzA were co-incubated with either H-89 (PKA inhibitor) or ESI-05 (EPAC inhibitor). The results demonstrated that GLP-1 secretion was negated in cells treated with the PKA inhibitor, but not in those treated with the EPAC inhibitor (Figure 2

(c)). PKA activity and <sup>Ser133</sup>CREB phosphorylation were also elevated (Figure 2(d,e)). In cells with siRNA-mediated reduction of Olfr544 expression, Olfr544 mRNA expression was reduced by 60%, compared to control cells transfected with scrambled shRNA (Figure 3(a)). AzA induced cAMP, PKA activity, <sup>Ser133</sup>CREB phosphorylation, and GLP-1 secretion. However, these effects of AzA were completely abrogated in cells with reduced expression of Olfr544 (Figure 3(b-d)). Taken together, these results showed that activation of Olfr544 by AzA induces GLP-1 secretion in L cells by stimulating the cAMP-PKA-CREB signaling axis in a cell autonomous manner.

### Gut microbiome analysis in HFD-fed mice

Activation of Olfr544 in gut could affect gut microbiota to regulate adiposity and inflammation,<sup>17</sup> thus we examined gut microbiota in HFD-fed



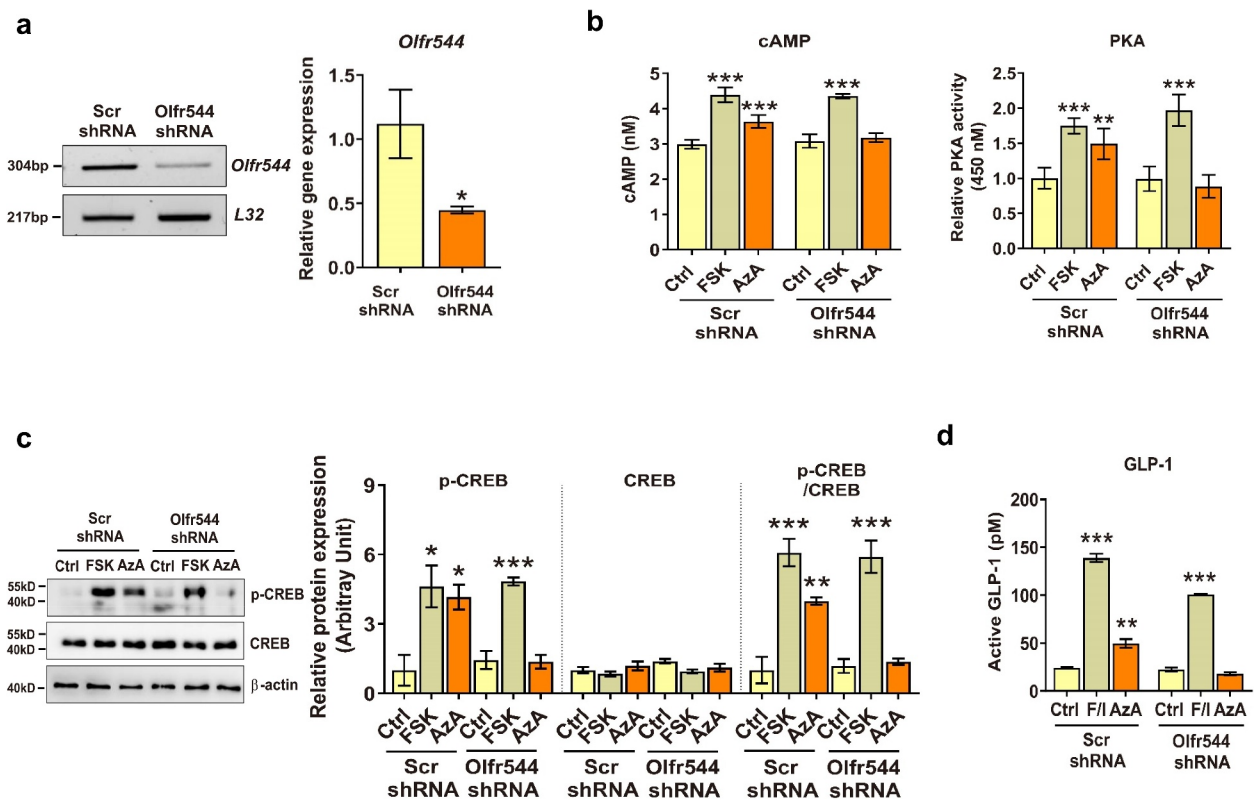


**Figure 3.** Silencing *Olf544* expression abrogates the effect of AzA on GLUTag cells. (a) *Olf544* knockdown in GLUTag cells transfected with shRNA against *Olf544*. The mRNA level of *Olf544* was determined by RT-PCR analysis ( $n = 3$ ). (b) Intracellular cAMP levels ( $n = 4$ ) and PKA activity ( $n = 4$ ) in GLUTag cells with *Olf544* gene knockdown. (c) CREB, p-CREB expression, and p-CREB/CREB ratio ( $n = 3$ ), and (d) GLP-1 secretion levels in GLUTag cells with *Olf544* gene knockdown ( $n = 3$ ). Scr, scrambled shRNA; Ctrl, control; F/I, 10  $\mu$ M forskolin and 10  $\mu$ M IBMX; FSK, forskolin (10  $\mu$ M); AzA, azelaic acid (50  $\mu$ M). The data are presented as the mean  $\pm$  SEM. One-way ANOVA followed by Tukey's HSD test and Student t-test were performed for multiple- and two group comparisons. \* $P < .05$ , \*\* $P < .01$ , \*\*\* $P < .001$  compared with controls.

mice. Gut microbiome analysis was performed in mice fed a HFD that were orally administered AzA for 8 weeks. AzA reduced the body weight of WT mice fed a HFD by 15% but not of *Olf544*-KO mice fed a HFD (Supplementary Figure 4(a, b)). The weights of epididymal, inguinal white adipose tissue, interscapular brown adipose tissue, and liver, were significantly reduced in mice fed a HFD that were administered AzA compared with controls without AzA treatment. However, body weight and fat tissue weight were unchanged by AzA in *Olf544*-deficient mice (Supplementary Figure 4(a, b)).

The microbiota comparison between WT and *Olf544*-KO mice are shown in Supplementary Figure 4c. Alpha diversity in WT and *Olf544*-KO mice (no AzA administration) was comparable. These results indicate that the microbiomes in WT control and *Olf544*-KO control groups are similar.

In microbiome analysis, AzA did not exert significant difference of alpha or beta diversity alpha or beta diversity in fecal microbiota, and cecal microbiome in both WT and *Olf544*-KO mice (Supplementary Figure 4(c, d)), however, AzA administration significantly altered specific members of the fecal microbiome in WT mice compared with those in *Olf544*-KO mice, including *Parabacteroides* ( $P = .003$ ), *Muribaculaceae* ( $P = .038$ ) (formerly known as the S24-7), *Oscillospira* ( $P = .028$ ), *Ruminococcus* ( $P = .038$ ) and *Clostridiales* (Figure 4 (a, b) and Supplementary Figure 4(e, f)). Notably, *Bacteroides acidifaciens* ( $P = .049$ ) was significantly enriched in the AzA administrated WT mice (Figure 4(b)); the gut commensal *B. acidifaciens* contributes to the prevention of obesity through regulation of GLP-1 levels in the gut<sup>18</sup> and the increased abundance of *B. acidifaciens* was found

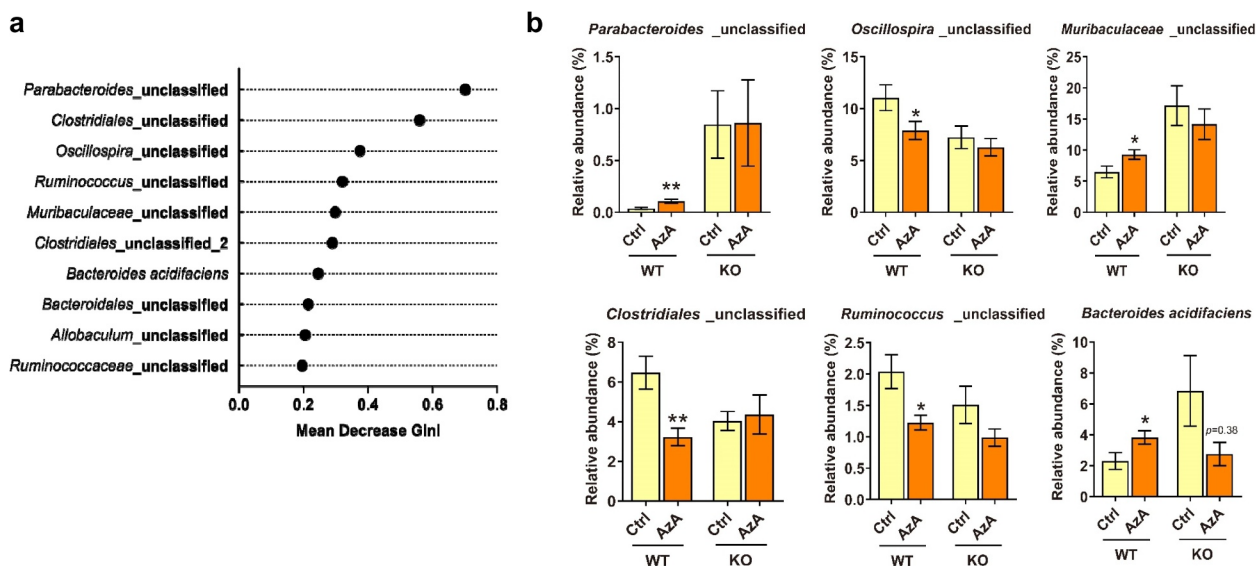


**Figure 4.** Fecal microbiome analysis of HFD-fed mice with 8 weeks Aza administration ( $n = 8$ ). (a) Top-10 features to discriminate Aza treatment from microbiome species-level dataset of wild-type mice, as measured by random forest method. (b) Comparison of relative abundances of significantly different microbial taxa at species level. Ctrl, control; Aza, azelaic acid (50 mg/kg body weight/day). Data are presented as mean  $\pm$  SEM. \*  $P < .05$ , \*\*  $P < .01$  by Mann-Whitney U test.

in interventions for obesity and glucose control.<sup>19,20</sup> These changes were nearly disappeared in Olfr544-KO mice with Aza oral administration.

To predict alterations of microbial function by Aza treatment, we inferred microbial function using the PICRUSt2 pipeline<sup>21</sup> in both WT and Olfr544-KO mice. Metabolic pathways of microbiota related to an antioxidant such as several types of ubiquinone biosynthesis and formaldehyde oxidation ( $P = .038$ ) were also enriched in Aza administrated WT mice (Supplementary Figure 5). These changes were all negated in Olfr544-KO mice. These results suggested that long-term Olfr-544 activation by Aza did not affect gut microbiome dramatically, however, alters specific members of the gut microorganisms related to anti-obesity and antioxidative effects.

### Fecal metabolome analysis in HFD-fed mice

Next, we investigated fecal metabolome altered by Aza in mice. First, the levels of Aza was measured in mice. Aza can be endogenously synthesized in tissues. Levels of Aza were elevated in the liver and adipose tissues, particularly in the fasting state (Supplementary Table 1). These suggest that endogenous Aza may function as an auxiliary fasting

signal by activating Olfr544 to stimulate white adipose tissue (WAT) lipolysis and hepatic fatty acid oxidation. Aza levels in feces were significantly higher in Aza administrated mice (Supplementary Table 1). These observations suggested that endogenously produced Aza in fasting and oral intake of Aza can activate Olfr544 in the gut.

In fecal metabolome analysis, 83 metabolites, including Aza, were identified and quantified using GC/TOF-MS (Supplementary Table 2). The Top 10 most significantly elevated metabolites in the Aza group of WT mice were Aza, norvaline, succinate, trehalose, uric acid, arachidic acid, cellobiose, O-phosphorylethanolamine, oxoproline, and glutamate (Supplementary Table 2); however, the levels of these metabolites except Aza became similar in both control and Aza groups in Olfr544-KO mice (Supplementary Table 2).

Principal component analysis, including key organic acids and amino acids revealed that metabolite profile of WT and Olfr544-KO mice were localized closely, indicating that the fecal metabolite profiles of WT and Olfr544-KO mice are comparable (Supplementary Figure 6). To examine the changes in metabolism in the gut environment by Aza, MetaMapp and the metabolite sets enrichment analysis (MSEA) were performed in WT and

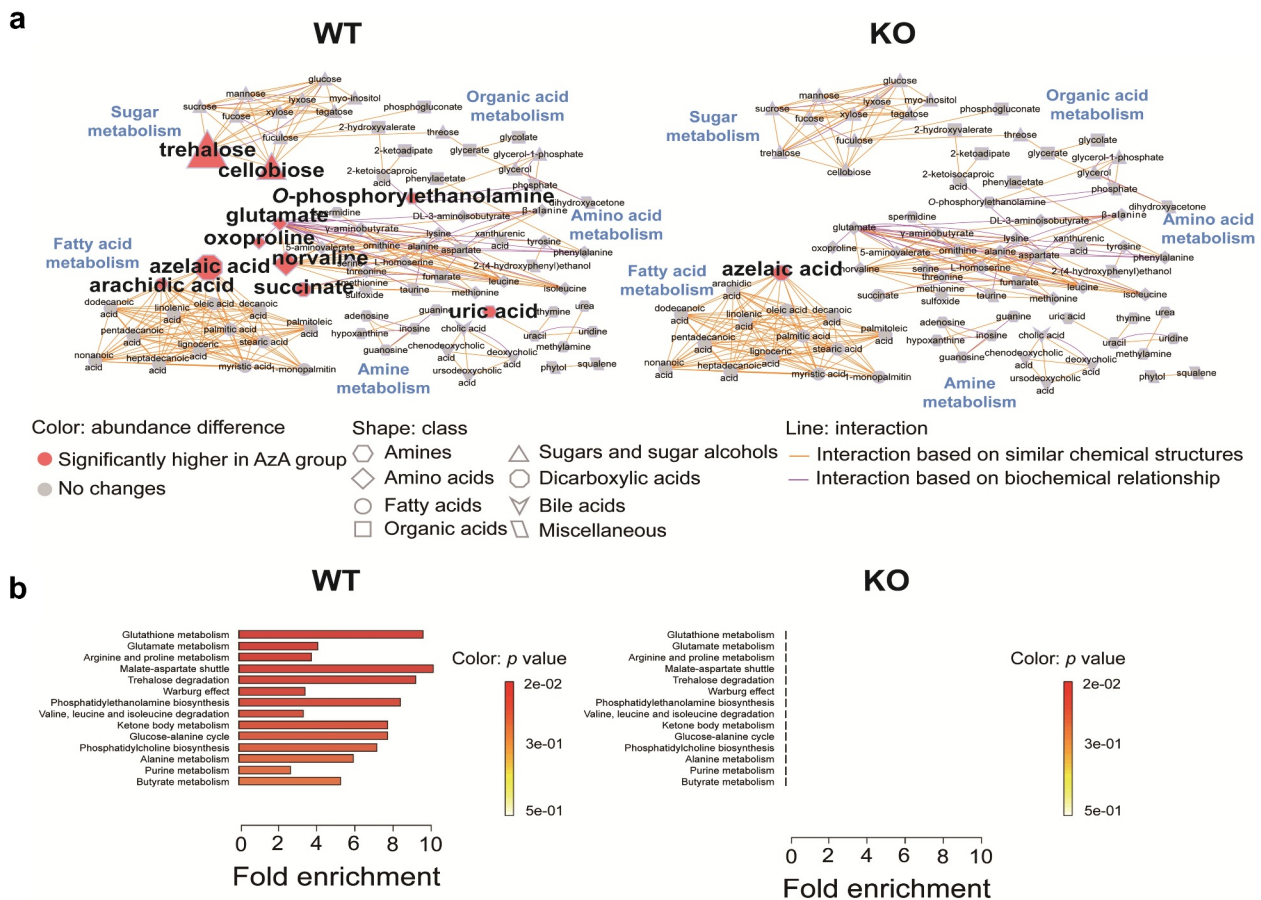


**Figure 5.** Fecal metabolome analysis of HFD-fed mice with AzA. (a) MetaMapp analysis of the fecal metabolites; Chemical classes of metabolites are represented by shapes. Significant changes in the abundance of metabolites are indicated by colors ( $P < .05$ , based on the Mann-Whitney U test). Magnitudes of fold changes are represented by the sizes of symbols; structural and biochemical similarities are represented by Orange and purple edges, respectively. Interactions based on similar chemical structures were calculated by using Tanimoto chemical and NIST mass spectral similarity scores; Interactions based on biochemical relationship were calculated by using KEGG reactant pair database. (b) Metabolite set enrichment analysis ( $n = 9$ ).

Olf544-KO mice orally administered with AzA (Figure 5(a,b)). Notably, results suggested that AzA administration significantly increased the levels of norvaline, succinate, trehalose, and O-phosphorylethanolamine in WT mice, but not in Olf544-KO mice (Figure 5(a)). Norvaline was correlated with significantly increased levels of glutamate and oxoproline, the intermediates of glutathione metabolism.<sup>22</sup> AzA also elevated the levels of 6-phosphogluconate, a key metabolite in the pentose phosphate pathway, which supplies NADPH to anabolism.<sup>23</sup> Succinate is known to be secreted by *B. acidifaciens*. Trehalose is a stress-resistance compound that is synthesized by microorganisms in a stressed environment, such as

under oxidative stress and heat shock.<sup>24</sup> O-phosphorylethanolamine is a metabolite in phospholipid synthesis for cell growth. These findings suggest that AzA affects survival and the proliferation of certain gut microorganisms with increased trehalose, phospholipid, succinate, and glutathione synthesis. Induced glutathione and NADPH synthesis may enhance antioxidative capacity in gut.

AzA administration showed significant correlations with specific gut microorganisms such as *Bacteroides acidifaciens*, *Parabacteroides*, *Muribaculaceae*, *Clostridiales*, and *Oscillospira* in HFD-fed WT mice. These results suggest that activation of Olf544 increases antiobesogenic gut

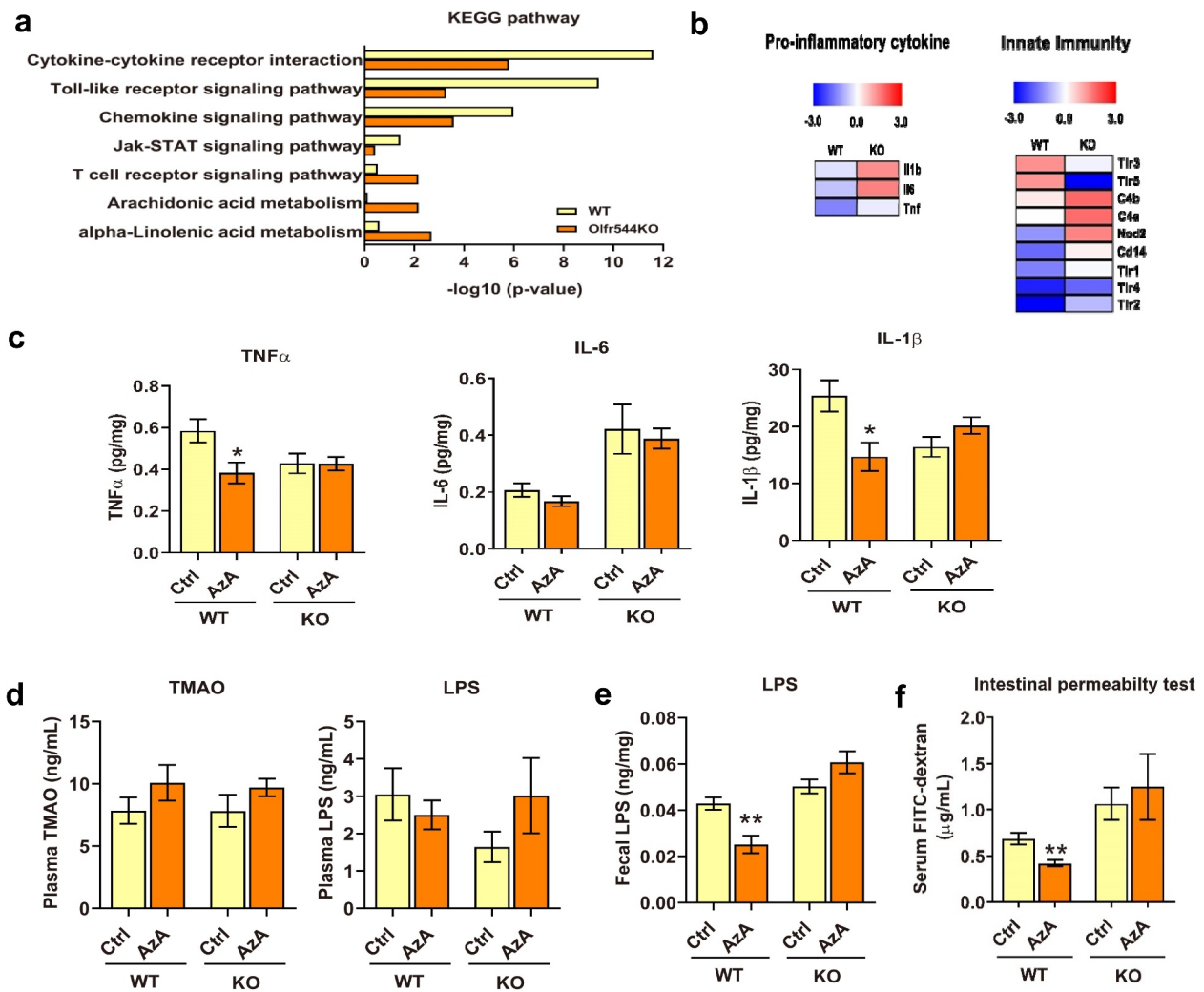


**Figure 6.** Anti-inflammatory effects of Olfr544 activation on mouse colon. (a) The KEGG pathway enrichment analysis using 320 genes shows affected pathways by AzA in the RNA-Seq analysis of LPS-stimulated colonic tissue explants isolated from WT and Olfr544-deficient mice. The bar graph shows the  $-\log_{10} P$  values for the enriched KEGG pathways. (b) Heat map shows that significantly up- and down-regulated genes by AzA in immune and inflammatory pathways in mice. (c) The colon levels of pro-inflammatory cytokines, (d) plasma trimethylamine N-oxide (TMAO) and lipopolysaccharide (LPS) levels, (e) fecal LPS levels in HFD-fed mice. (f) Intestinal permeability test in HFD-fed WT and Olfr544-KO mice ( $n = 5-6$ ). Ctrl, control; AzA, azelaic acid (50 mg/kg body weight/day). The data are presented as the mean  $\pm$  SEM. \* $P < .05$ , \*\* $P < .01$ , by Student's t test for comparison of 2 groups.

microorganisms and metabolites such as *B. acidifaciens* and succinate and these fecal changes may at least in part contribute to the anti-obesogenic effects of Olfr544 activation.

#### Transcriptome profiling indicates suppression of pro-inflammatory gene network in mouse colonic tissue explants treated with AzA

RNA-Seq analysis was performed in lipopolysaccharide (LPS)-stimulated colonic tissue explants isolated from WT and Olfr544-KO mice. KEGG pathway analysis with 650 transcripts that showed

2-fold induction/reduction by AzA treatment revealed that AzA significantly regulated the expression of genes involved in the several inflammation pathways including cytokine-cytokine receptor interaction, toll-like receptor and chemokine signaling pathways; these changes were largely abrogated in colonic tissues from Olfr544-KO mice (Figure 6(a)). The expression levels of pro-inflammatory cytokines TNF- $\alpha$ , IL-1 $\beta$ , and IL-6 were reduced by AzA in LPS-stimulated WT colonic tissues; corresponding changes were largely negated in colonic tissues from Olfr544-KO mice (Figure 6(b)). Similarly, the changes in gene expression in innate immunity by



AzA in WT mice were either disappeared or reversed in Olf544-KO mice. AzA tended to reduce pro-inflammatory cytokine expression, but the effect was non-significant in colonic explants without LPS treatment (Supplementary Figure 7). RNA-Seq analysis of GLUTag cells showed similar activation of the anti-inflammatory activity of Olf544 following treatment with AzA (data not shown). These results indicated that AzA significantly suppressed pro-inflammatory signaling pathways, particularly those related to TNF and related genes, in *ex vivo* colonic tissues dependent on Olf544.

### **AzA inhibits expression of pro-inflammatory cytokines in HFD-fed mouse colon**

We finally investigated the anti-inflammatory effects of Olf544 activation in gut of HFD-fed mice. Gut inflammation is a key feature found in obesity.<sup>25</sup> AzA significantly reduced the TNF- $\alpha$  and IL-1 $\beta$  levels with marginal effects on IL-6 levels in colon tissues of HFD-fed WT mice (Figure 6(c)). However, these effects were disappeared in Olf544-KO mice. Fecal LPS levels were similar between WT and Olf544-KO mice at baseline. However, long-term AzA administration reduced fecal LPS concentration, with marginal effects on plasma TMAO and LPS levels in WT mice. These effects of AzA on fecal LPS were negated in Olf544-KO mice (Figure 6(d,e)). The gut barrier plays a key role in the reduction of inflammatory responses to the microbiota; it is regulated by a finely tuned network of immune mechanisms for microbial recognition and tolerance to the microbiota.<sup>26,27</sup> Accordingly, we examined the effects of AzA administration on intestinal permeability, which reflects intestinal inflammation or impaired intestinal functions. Gut permeability was higher in Olf544 deficient mice compared with WT mice. The results showed that AzA administration significantly reduced intestinal permeability in HFD-fed WT mice, whereas these effects were negated in HFD-fed Olf544-KO mice (Figure 6(f)); thus, AzA administration appears to reduce intestinal inflammation and improve intestinal function in an Olf544-dependent manner.

## **Discussion**

The olfactory receptor Olf544 is ectopically expressed in multiple tissues in mice. In this study, we investigated the biological functions of Olf544 in the gut, focusing on enteroendocrine regulation and inflammation. AzA induced GLP-1 secretion in mice, both *ex vivo* and *in vivo*. In GLUTag L cells, AzA activated the cAMP-PKA-CREB signaling axis and induced GLP-1 secretion. The induction of GLP-1 by AzA was diminished in GLUTag cells with reduced expression of Olf544, as well as in Olf544-KO mice. These findings demonstrated that the induction of GLP-1 secretion by AzA is cell autonomous and Olf544-dependent. Gut microbiome analysis revealed that, although AzA did not markedly alter microbiota diversity, it increased levels of marker microorganisms for leanness, including *B. acidifaciens*. AzA reduced the levels of LPS in fecal samples, as well as levels of pro-inflammatory cytokines (e.g., TNF- $\alpha$  and IL-1 $\beta$ ) in colonic tissues, thus improving intestinal permeability. These effects of AzA were all abrogated in Olf544-KO mice. Taken together, these findings showed that Olf544 plays a major role in the gut through induction of GLP-1 secretion, modulation of obesity marker gut microorganisms, and suppression of pro-inflammatory cytokine and LPS production in the gut.

AzA enhanced plasma GLP-1 concentrations in mice. The intestinal tract is the largest endocrine organ; it plays important roles in regulating metabolic homeostasis throughout the body.<sup>28</sup> L cells, which secrete GLP-1, GLP-2, and PYY, are primarily located in the distal gut, ileum, and colon.<sup>28</sup> However, Olf544 activation by AzA had no effect on GLP2 and PYY secretion in WT mice. Recent studies have demonstrated several functions of GLP-1 in the regulation of insulin sensitivity, energy metabolism, and anti-inflammatory effects.<sup>29</sup> Thus, GLP-1 and GLP-1 receptor agonists have been suggested as novel therapeutic agents for weight loss;<sup>30</sup> the GLP-1 analogue, liraglutide, has been approved as an injectable anti-obesity drug and is one of the most potent anti-obesity drugs available.<sup>31</sup> We demonstrated that AzA induced GLP-1 secretion with anti-obesogenic effects in

mice; these results suggest that body fat reduction by AzA may be at least partially mediated by GLP-1 secretion in the gut.

An understanding of the mechanism underlying GLP-1 secretion is especially important for the treatment and prevention of metabolic diseases, such as obesity and Type II diabetes. GLP-1 secretion is known to require intracellular calcium signaling in several nutrient-sensing mechanisms in L cells. Glucose stimulates GLP-1 secretion through the closure of ATP-sensitive potassium channels,<sup>32</sup> thereby increasing intracellular calcium levels. *In vivo* and *ex vivo* studies have demonstrated that glucose induces GLP-1 release through the sodium-glucose cotransporter SGLT1 and -to a lesser extent- the glucose transporter GLUT2.<sup>33</sup> Activation of FFAR2, a short-chain fatty acid receptor, induces GLP-1 secretion by increasing intracellular calcium concentrations through the  $G_{H\Omega}$  signaling pathway.<sup>34</sup> GPRC6A, an amino acid receptor, stimulates GLP-1 secretion through the induction of intracellular calcium concentration.<sup>35</sup> Lysophosphatidyl inositol induces activation of the TRPV2 channel and increases intracellular calcium levels to trigger GLP-1 secretion.<sup>36</sup> The bitter tastant quinine modulates GLP-1 exocytosis *via* actin reorganization through elevation of intracellular calcium concentrations,<sup>37</sup> suggesting the involvement of ectopic bitter taste receptors in regulation of GLP-1 secretion in L cells.

In addition, the cAMP-PKA signaling pathway has been implicated in GLP-1 secretion in L cells.<sup>38,39</sup> Inhibitors of PDE4, which degrades cAMP, have been shown to improve glucose homeostasis in diabetic mice, potentially by enhancement of cAMP-mediated GLP-1 secretion.<sup>40</sup> Adrenaline is known to stimulate GLP-1 secretion in L cells; this hormone increases both intracellular calcium and cAMP concentrations. Induction of cAMP and GLP-1 exocytosis were reportedly blocked by a  $\beta$ 1-adrenalin receptor inhibitor.<sup>39</sup> The results of the present study further demonstrated that Olfr544 activation specifically induces the cAMP-PKA-CREB signaling pathway, but does not affect intracellular calcium levels, to stimulate GLP-1 secretion in L cells. These findings add novel information regarding the GLP-1 secretion mechanism that AzA mediates GLP-1 secretion by PKA stimulation in the gut.

Modulation of gut microbiota composition could offer therapeutic strategies for metabolic diseases, such as obesity and Type II diabetes. AzA did not cause marked changes in the gut microbiota, although the dominant species and families of the gut microorganism population were altered by AzA administration. Importantly, the abundances of the genus *Parabacteroides* and the species *B. acidifaciens* were significantly elevated in AzA-treated mice; these changes were negated in Olfr544-KO mice, indicating that these effects were due to activation of Olfr544 in the gut, and not to AzA itself, although the underlying mechanism is not yet clear. *B. acidifaciens* was first isolated from the mouse cecum.<sup>41</sup> This novel commensal gram-negative anaerobic bacterium is characterized by growth in bile acid, esculin hydrolysis, and glucose 6-phosphate dehydrogenase and 6-phosphogluconate dehydrogenase activities.<sup>41</sup> The induction of *B. acidifaciens* is of interest, because this strain alters the gut commensal bacteria community, thereby improving lipid and glucose metabolism and modulating the levels of GLP-1 in mice.<sup>18-20,42</sup> We found that *B. acidifaciens* levels were elevated in AzA-fed mice, which suggests that AzA significantly increases the population of marker gut microorganisms for leanness.

*B. acidifaciens* levels were increased in Olfr544-deficient mice compared with WT mice. In Olfr544-KO mice, the possibility that a lack of unknown Olfr544-dependent host-microbe interactions causes microorganism population changes cannot be excluded. In addition, AzA possibly increases *B. acidifaciens* to compensate anti-obesity signaling mediated by Olfr544 in Olfr544-KO mice. These results will be further investigated in future studies.

The increase in *B. acidifaciens* due to AzA administration may contribute to the prevention of obesity through changes in the fecal metabolome. In addition, microbiota associated with antioxidant metabolism were also increased by AzA. In metabolomic analysis, succinate and trehalose were simultaneously increased in AzA-treated mice. Succinate is a metabolite actively secreted by *B. acidifaciens* in the intestine<sup>41</sup> and plays a role in preventing obesity and insulin resistance.<sup>43</sup> The changes in gut microbiome and metabolome and prevention of obesity by AzA administration were

not found in *Olf544*-KO mice. Therefore, AzA administration may contribute to the prevention of obesity through changes in specific gut microorganisms and the fecal metabolome.

AzA administration significantly increased fecal levels of succinate in WT mice fed a HFD but not in *Olf544*-KO mice fed a HFD. Succinate is an intermediate in the citric acid cycle and in the microbial synthesis of propionate, which reportedly has complex functions regarding regulation of adiposity. Alternatively, succinate in the gut is sensed by its cognate receptor, SUCNR1, activating diverse signaling pathways having several functional effects including regulation of microbiota-triggered Type II immunity, which may affect gut inflammation and intestinal permeability.<sup>44</sup>

The succinate levels in the gut are increased in mice with a high dietary fiber diet and is secreted by *B. acidofaciens*. Increased succinate levels in the gut resulted in the activation of intestinal gluconeogenesis, which prevented the obese and glucose-intolerant phenotype of mice fed a high-fat high-sucrose diet.<sup>45</sup> Similar results have been reported showing dietary fibers, such as arabinoxylan, increased succinate production in a culture of mixed gut microorganisms.<sup>46</sup> However, the fecal levels of succinate are positively associated with body weight.<sup>47</sup> Thus, whether succinate represents a microbial-derived obesity-preventing metabolite or is a metabolite marker of obesity remains to be determined.

Trehalose is a functional disaccharide with several metabolic functions, such as suppression of inflammatory responses.<sup>48,49</sup> The anti-obesity effect of trehalose has been reported. Trehalose suppressed adipocyte hypertrophy and alleviation of impaired glucose tolerance.<sup>50</sup> In addition, oral administration of trehalose reportedly induces beige adipogenesis and thermogenesis and reduces white adipocyte size; thus, trehalose is considered a thermogenic dietary compound.<sup>51</sup> Trehalose also induces antioxidative and lysosomal gene expression, resulting in reduced cellular reactive oxygen species in adipose tissues.<sup>52</sup> In addition, trehalose has been shown to activate hepatic Alox3, which results in the reduction of weight gain and hepatic steatosis, thus ameliorating metabolic disease.<sup>53</sup> These results collectively indicate that trehalose may have anti-obesogenic effects in multiple organs after uptake by the intestine.

The anti-inflammatory effects of GLP-1 and GLP-1 analogues have been explored in different tissues, including the colon.<sup>54,55</sup> Furthermore, the gut microbiota contributes to obesity-induced chronic-low grade inflammation. CREB activation directly suppresses pro-inflammatory responses by inhibition of NF- $\kappa$ B activation. Long-term AzA administration reduced fecal LPS levels and intestinal permeability in HFD-fed mice, indicating that AzA administration reduces intestinal inflammation and improves intestinal functions in HFD-mice. The anti-inflammatory effects of *Olf544* activation by AzA may be mediated by the combined effects of CREB activation, GLP-1 regulation, and/or production of LPS by gut microbiota.

AzA is endogenously produced in cells by  $\omega$ -oxidation of medium-chain fatty acids.<sup>56</sup> AzA is a C9-dicarboxylic acid present in the hulls of grains, including oat, barley, and wheat.<sup>57</sup> Notably, AzA is a potent ligand for *Olf544*.<sup>5,7</sup> The results of the present study indicated that cellular AzA levels were particularly elevated in the fasting state, suggesting a potential role for AzA as an auxiliary regulator of fasting energy metabolism. In addition, AzA has anti-inflammatory activity and has been used as a pharmacological agent, especially for the treatment of inflammatory skin diseases, acne, and rosacea.<sup>11</sup> However, the target protein for AzA has not been unknown. It is possible these anti-inflammation by AzA may be mediated by *Olf544* as well and further studies are necessary to examine these possibilities. Our results indicate that AzA did not exert significant anti-inflammatory effects in the normal colons of mice but the effects were exaggerated in colons of mice treated with LPS under stress conditions. AzA showed significant anti-inflammatory effects with LPS treatment, a stressed condition of inflammation but AzA effect was marginal in gut without LPS treatment.

Intestinal permeability of *Olf544*-KO mice were higher than those WT mice while plasma and fecal LPS levels were not increased in *Olf544*-KO mice. Mechanism of increase intestinal permeability and the levels of *B. acidofaciens* in *Olf544*-KO mice will be investigated in the future.

In conclusion, we explored the novel effects of *Olf544* activation by AzA in the gut. *Olf544* activation contributes to activation of the cAMP-PKA-

CREB signaling axis, thus increasing GLP-1 levels and suppressing anti-inflammatory cytokines. The anti-inflammatory activity of AzA contributes to improved gut permeability. Modulation of the gut metabolome and microbiota in small intestine and colon tissues may contribute, at least partially, to the anti-obesogenic and anti-inflammatory effects of Olfr544 activation. These results suggest a novel mechanism of action of ectopic ORs in the gut with respect to regulation of metabolism and inflammation.

## Methods and materials

### Cell culture and reagents

GLUTag cells were kindly provided by Prof. Daniel Drucker (University of Toronto, Toronto, ON, Canada) and Prof. Toru Hira (Hokkaido University, Sapporo, Hokkaido, Japan). The cells were cultured in DMEM/low glucose (HyClone, Logan, UT, USA) with 10% FBS (HyClone, USA), 1% penicillin/streptomycin (PEST, Welgene Inc., Korea) and 1% GlutaMAX (Gibco, MD, USA). AzA was purchased from Sigma-Aldrich (St. Louis, MO, USA), forskolin was obtained from Abcam (Seoul, South Korea), and 3-isobutyl-1-methylxanthine (IBMX) was purchased from Cayman (MI, USA). Primary antibodies against  $\beta$ -actin (SC-47778, 1:1000),  $\alpha$ -tubulin (SC-5286, 1:1000), CREB (SC-377154, 1:500), *p*-CREB (Ser133; SC-101663, 1:500) were obtained from Santa Cruz Biotechnology (Santa Cruz, CA, USA). Anti-mouse (31430) and anti-rabbit (31460) immunoglobulin G secondary antibodies (1:5000) were from Invitrogen (Carlsbad, CA, USA). Antibodies were used in immunoblot analyses with the referred dilution in the parenthesis.

### Mouse experiments

Healthy 6 to 8-week-old male C57BL/6 J wild-type (WT) mice were obtained from Samtako (Gyeonggi-do, Korea). Olfr544 deficient mice were constructed previously.<sup>5</sup> All animal experiments were conducted according to protocols approved by the Animal Experiment Committee of Korea University (Protocol No. KUIACUC-2019-97 and 2019-0031). Mice were maintained under a 12-h

photoperiod, at a temperature of 21–25°C and a relative humidity of 50–60%. The mice were fed on 60% high fat diet (HFD) for 4 weeks and subsequently randomly assigned into the test or vehicle group. HFD used in this study is rodent diet containing 60% of calories from fat (D12492, Research Diets, Inc). The mice were fed with an HFD and 0.05% (w/w) AzA for 6 weeks or an HFD and orally administered AzA (50 mg/kg body weight) for 8 weeks. The former feeding was to confirm anti-obesogenic effects of AzA in diet and the latter was to investigate microbiome and metabolomic analyses. The mice in the vehicle group were administered ddH<sub>2</sub>O. The body weight and food intake of the mice were measured twice a week. Mice were fasted overnight before being sacrificed. Blood was collected in EDTA tubes (BD Vacutainer) retro-orbitally or by cardiac puncture, centrifuged at 300 ×g for 20 min at 4°C to separate plasma, and stored at –80°C. Liver and epididymis adipose tissues were collected, frozen in liquid nitrogen, and stored at –80°C until analysis. Blood triglyceride, total, LDL, HDL cholesterol levels, AST, and ALT levels, thyroid hormone levels were analyzed by Cobas 111 autoanalyzer using enzymatic methods. Mouse hepatic triglyceride concentrations were quantified as previously.<sup>5</sup> Briefly, 15 mg of mouse livers were weighed and homogenized in 600  $\mu$ L of acetone (Deajung, Seoul, Korea), then the samples were agitated and incubated at 4°C overnight. The lipid contents were collected through centrifugation at 12000 ×g for 10 min at 4°C. The samples were then dried and dissolved in 95% ethanol. Hepatic triglyceride concentrations were measured using Cobas C111 autoanalyzer (Roche, Basel, Switzerland) and normalized to the liver weight.

### Measurements of second messengers, PKA activity, cell proliferation, mitochondrial biogenesis, and apoptosis in GLUTag cells

GLUTag cells were seeded for 2 d and then treated with 50  $\mu$ M AzA or 10  $\mu$ M forskolin for 15 min and 30 min for cAMP measurement and PKA activity assay, respectively. cAMP concentrations were assayed using a fluorimetric ELISA kit (AAT Bioquest, Sunnyvale, CA, USA). PKA kinase activity was measured using a commercial kit from Enzo Life Science (Farmingdale, NY, USA). Intracellular



calcium was quantified with Fluo-4 Direct Ca<sup>2+</sup> reagent (Invitrogen, USA), and inositol phosphates were measured with a HTRF IP-one Tb kit (Cisbio, Bedford, MA, USA), according to the manufacturer's protocol. Cell proliferation was analyzed using the CellTiter-Glo 2.0 kit (Promega, Madison, WI). Mitotracker Green probe (Molecular Probes) was used to measure the mitochondrial biogenesis in GLUTag cells following the manufacturer's instructions. Briefly, GLUTag cells were incubated with Green probes (200 nM) for 30 min at 37°C after washing with PBS (pH 7.4). Subsequently, the green fluorescence intensity was measured using SpectraMAX (Molecular Devices Co.) at the wavelength of 490 nm (excitation) and 516 nm (emission), respectively. Apoptosis assay was performed in GLUTag cells at 24 h post treatment using the Caspase-Glo 3/7 assay kit (Promega) according to the manufacturer's instructions.

#### **RT-PCR and qPCR analysis**

The total RNA was isolated using RNAiso Plus reagent (Takara Bio Inc., Otsu, Japan) from tissues and cells. The cDNA was synthesized by using a ReverTra Ace<sup>®</sup> RT Master Mix kit (Toyobo, Osaka, Japan) according to the manufacturer's instructions. RT-PCR was performed with EmeraldAmp<sup>®</sup> GT PCR Master Mix reagent according to the manufacturer's instructions. The RT-PCR products were analyzed by agarose gel electrophoresis (4%) and image analysis were obtained by using a ChemiDoc touch imaging system with the Image Lab 5.2 software (Bio-Rad, Redmond, WA, USA). The qPCR was performed with the Thunderbird<sup>™</sup> SYBR<sup>®</sup> qPCR Mix reagent (Takara Bio Inc., Otsu, Japan) and iQ5 Cyclor System (Bio-Rad, Hercules, CA, USA). Amplification was performed using an initial denaturation step at 95°C for 3 min, followed by 40 cycles of denaturation at 95°C for 20 s, annealing at 60°C for 30 s, and extension at 68°C for 1 min. The fluorescent signal was quantified automatically at the end of each PCR cycle. The expression levels were normalized to the levels of L32 and GAPDH for qPCR and RT-PCR, respectively. GAPDH and L32 are genes encoding glycolysis and ribosomal protein, respectively, of which gene expression is

stably expressed in multiple cell types thus considered as one of the most stably expressed house-keeping genes in mammalian cells.<sup>58</sup> Oligonucleotide sequences are given in Supplementary Table 3.

#### **Immunoblot analysis**

Total proteins from cultured cells and mouse tissues were extracted as described previously.<sup>5</sup> Briefly, proteins were extracted using radioimmunoprecipitation assay (RIPA) buffer supplemented with Halt protease and phosphatase inhibitor reagent (Thermo Fisher Scientific, CA, USA). The samples were then centrifuged for 10 min at 13,000 rpm at 4°C. Protein concentration was determined with a series of bovine serum albumin standards (Bovogen Biologicals, Melbourne, Australia) and Bio-Rad reagent (Bio-Rad, USA). The denatured proteins were separated on an SDS-PAGE gel (10%) and transferred to nitrocellulose membranes (Daeillab, Seoul, Korea). The membranes were blocked for 1 h in TBS with 5% (w/v) nonfat dried milk and probed with specific antibodies overnight at 4°C in TBS with 0.1% Tween-20 and 5% nonfat dried milk. Immunoblot images were obtained with a ChemiDoc touch imaging system and analyzed with the Image Lab 5.2 software (Bio-Rad). Protein expression levels were normalized to  $\beta$ -actin or  $\alpha$ -tubulin expression.

#### **Olf544 knockdown**

Olf544 gene knockdown was performed according the previously reported method.<sup>5</sup> Oligonucleotides encoding shRNA hairpin sequences targeting Olf544 (top strand: 5'-CACCGCTCACTGTTCGCATCTTCATTCGAAAATGAAGATGCGA-ACAGTGAG-3') or encoding nontargeting scrambled shRNA hairpins (top strand: 5'-CACCGTAAGGCTATGAAGAGATACCGAAGTATCTCTTCATAGCCTTA-3') were inserted into the shRNA cloning site of the pENTR/U6 vector using the Block-iT U6 RNAi entry vector kit (Invitrogen, USA). GLUTag cells were seeded in 24-well plates for 2 d. At 60–70% confluence, cells were transfected with 0.625  $\mu$ g of either scramble or Olf544 shRNA using

Lipofectamine 2000 (Invitrogen) following the manufacturer's instructions. After 4 h of initial transfection, GLUTag cells were transfected again with scramble or Olfr544 shRNA at the same concentration. After 5 h of double transfection, 1 mL of fresh medium containing 20% FBS (Hyclone) was added, and the cells were incubated for 18 h before treatment.

### **Measurement of GLP-1 level**

GLP-1 was measured in cultured GLUTag cells and mouse *ex vivo* and *in vivo*. GLUTag cells were seeded in culture medium for 2 d, and GLP-1 levels were measured as described previously.<sup>38</sup> Cells were washed with glucose-free Krebs-Ringer bicarbonate buffer and incubated for 30 min in the same buffer containing 100  $\mu$ M dipeptidyl-peptidase (DPP)-IV inhibitor diprotin A (Abcam, USA), and 0.5% (w/v) bovine serum albumin. Cells were then treated with 30  $\mu$ M forskolin and 10  $\mu$ M IBMX, or AzA (50  $\mu$ M) for 2 h. For PKA or EPAC inhibitor assays, GLUTag cells were pre-treated with either 10  $\mu$ M H-89 (PKA inhibitor; Sigma-Aldrich), or 5  $\mu$ M ESI-05 (EPAC inhibitor; Sigma-Aldrich) for 1 h and further treated with 50  $\mu$ M AzA for an additional 1 h. The supernatants were collected after centrifugation for 5 min at 3,000 rpm. Active GLP-1 concentrations were measured by ELISA (Merck Millipore, USA), which was normalized to that of total protein concentrations. For *ex vivo*, GLP-1 secretion experiments were performed according to the previously reported methods.<sup>38,59</sup> C57BL/6 male mice were fed on a chow diet. The mice were sacrificed, and intestinal segments of 1 cm were first dissected, minced, and washed in PBS. The intestinal segments were then maintained in DMEM/high glucose 10% FBS containing 100  $\mu$ M diprotin A for 4 h and treated with 30  $\mu$ M forskolin and 10  $\mu$ M IBMX, or AzA (50  $\mu$ M) for 1 h. The supernatants were collected after centrifugation for 5 min at 3,000 rpm. The GLP-1 levels were measured by ELISA (Elabscience, USA), which was normalized to that of total protein concentrations. For *in vivo*, GLP-1 secretion experiments were performed as reported previously.<sup>38,60,61</sup> C57BL/6 male mice were fed a chow diet, then animals were i.p. injected with

100 mg/kg body weight AzA and a DPP-4 inhibitor, diprotin A (3 mg/kg; Abcam, Cambridge, USA) or vehicle (PBS). Blood was collected from the tail vein 1 h after injection and transferred to EDTA tubes containing diprotin A and protease and phosphatase inhibitor cocktail. Plasma was collected by centrifugation at 2,000 rpm for 30 min at 4°C. Active GLP-1 concentrations were then measured by ELISA (Merck Millipore, USA). GLP-1 levels were also measured in fasting mice after AzA oral administration. In this case, after 8-week of AzA administration (on 60% HFD), mice were sacrificed after overnight fasting then blood was collected for GLP-1 hormone analysis. Plasma was collected by centrifugation at 2,000 rpm for 30 min at 4°C. Active GLP-1 concentrations were then measured by ELISA (Merck Millipore, USA).

### **Measurement of PYY, GIP, GLP-2, and ghrelin levels**

In mice the PYY, GIP and ghrelin (Elabscience, USA), and GLP-2 (Cusabio, USA) were measured in plasma using commercially available kits using manufacturers' instructions.

### **Intestinal permeability assay**

Intestinal permeability was assessed using the FITC-dextran intestinal permeability test, which was conducted similar to as previously reported.<sup>62</sup> The mice were fasted overnight and received an oral gavage FITC-dextran (4 kDa, Sigma-Aldrich) dissolved in sterile PBS. The administered dose was 600 mg/kg body weight, and the approximate volume administered per mouse was 0.2 mL. The other animal was treated with a corresponding dose of PBS. Exactly two hours after the FITC-dextran was administered, approximately 100  $\mu$ L of whole blood was collected by tail vein. The blood was collected in an EDTA-coated tube and centrifuged (3,500 g, 15 min, 4°C), and the plasma was collected. Plasma FITC-dextran concentrations were assessed using black 96-well plates using a Spectramax i3x Plate reader (Molecular Devices) with excitation at 490 nm and emission at 520 nm. Concentrations were calculated from a standard curve.

### **Estimation of levels of pro-inflammatory cytokines in the colon**

Colon tissues were homogenized in ice cold RIPA buffer, followed by centrifugation at 13,000 rpm for 15 min at 4°C. The supernatants of the colon homogenate was collected, and total protein concentration was determined. The levels of pro-inflammatory cytokines TNF $\alpha$ , IL-1 $\beta$ , and IL-6 in supernatants were assayed using sandwich ELISA kits (Invitrogen, USA). The estimations were performed based on colorimetric detection according to manufacturer's protocol. The concentrations of TNF $\alpha$ , IL-1 $\beta$ , and IL-6 in each sample were calculated using kit-provided standards.

### **Trimethylamine-N-oxide (TMAO) and LPS measurements**

Fecal samples were collected 1 h after AzA administration at the end of long-term AzA administration, as previously described.<sup>63</sup> Briefly, 50 mg of dried pulverized feces were extracted in 1.0 mL of 75% ethanol for 2 h at 50°C. The samples were then centrifuged at 1,050 g for 10 min. And 100  $\mu$ L of supernatant was mixed to 500  $\mu$ L of PBS for further analysis. Plasma TMAO (Mybiosource) and plasma and fecal LPS (Cusabio) levels were measured using commercial ELISA kits according to the manufacturer's instructions, respectively.

### **Ex vivo cultures of colonic tissue explants and RNA sequencing**

The *ex vivo* cultures of colonic tissue explants was established according to the previously described methods with slight modifications.<sup>64</sup> Briefly, WT and Olf544-KO mice were sacrificed, and an area of the proximal colon was dissected, and the tissue was rinsed with PBS, and a section of colonic explants was maintained in a humidified cell culture incubator with 5% CO<sub>2</sub> at 37°C for 4 h, in DMEM buffer with added 10  $\mu$ g/mL of bacterial LPS (source: *Escherichia coli* strain B4). During the incubation period, tissues were treated with AzA (50  $\mu$ M). Total RNAs from either WT or Olf544-KO mouse colonic tissue explants were prepared using a Ribospin kit (GeneAll, Seoul,

Korea). Library construction, amplification, purification, and high-throughput sequencing were performed by means of single-end 75-bp sequencing using a NextSeq 500 (Illumina, San Diego, CA, USA) by Ebiogen (Seoul, Korea). For gene annotation enrichment analysis, genes were selected and input into the DAVID functional annotation tool (<https://david.ncifcrf.gov/>). Gene Ontology and KEGG pathway assignment were performed with DAVID v6.8.

### **16S rRNA gene sequencing**

The WT and Olf544-KO mice fed a 60% HFD were orally administered with AzA (50 mg/kg body weight) for 8 weeks as described in "Mouse experiments" section. Then, cecum and fecal samples from each mouse were collected in sterile tubes, immediately snap-frozen in liquid nitrogen, and stored at -80°C until the further use. Total DNA was collected from the feces and cecum using a QIAamp Fast DNA stool mini kit (Qiagen, Hilden, Germany), in accordance with the manufacturer's instructions. Cecum and fecal samples were homogenized with 5-mm stainless steel beads (Qiagen), then homogenized thoroughly with 0.1-mm glass beads. Illumina-adapted universal primers, 515 F/806 R, which target the V4 region of the 16S rRNA gene, were used for DNA amplification; the amplicons were then purified using a QIAquick PCR Purification Kit (Qiagen). Amplicons were pooled and sequencing was performed using a MiSeq platform (Illumina, San Diego, CA) to produce 300-bp paired-end sequences.

### **Cecal and fecal microbiota analysis**

Demultiplexed 2 x 300 sequencing reads were processed using QIIME 2 (v. 2020.2).<sup>65</sup> The DADA2 plugin<sup>66</sup> was used for quality filtering, de-noising, and removal of chimaeric sequences. Amplicon sequence variant (ASV)-based taxonomic classification was performed using a machine-learning classifier, trained on the V4 515–806 bp regions of 16S rRNA gene sequences from the Greengenes gg\_13\_8 reference database.<sup>67</sup> The functional potential of the microbiome was predicted using PICRUSt2.<sup>21</sup> The alpha diversity was determined

based on Observed features and Shannon indices calculated in QIIME 2. Non-parametric multi-dimensional scaling (NMDS) plots were generated using the *Vegan* package in (v. 2.5–6) R,<sup>68</sup> and the distance was measured using the Bray-Curtis methods. Important features for discriminating between groups were estimated using the *randomForest* (v. 4.6–14) R package.<sup>69</sup> 80% of the samples were used for training models and five-fold validations were performed using *caret* R package (v.6.0–86). Statistical significance was calculated using the Mann-Whitney U test or Kruskal-Wallis test in GraphPad Software.

### **GC/TOF-MS analysis of metabolites**

The WT and Olfr544-KO mice fed a 60% HFD were orally administered with AzA (50 mg/kg body weight) for 8 weeks as described in “Mouse experiments” section. Metabolites were extracted from fecal samples using the methanol extraction method with slight modifications.<sup>70</sup> Briefly, samples were thawed on ice, and 50 mg of each sample was transferred to a fresh 1.5-mL Eppendorf tube. Then, 1 mL of pure methanol (Merck Millipore, Burlington, MA, USA) was added to each sample. The mixture was homogenized using a needle, sonicated for 30 min, vortexed for 10 min, and centrifuged at  $16,100 \times g$  for 10 min at 4°C. The supernatant was filtered by using a syringe filter (0.20- $\mu\text{m}$  pore size; Thermo Fisher Scientific, Waltham, MA, USA). Aliquots of 500  $\mu\text{L}$  of the supernatant were dried under vacuum at room temperature.

Methoximation and silylation were performed for qualification and relative quantification of metabolites using GC/TOF-MS. For methoximation, 10  $\mu\text{L}$  of 40 mg/mL methoxyamine hydrochloride in pyridine (Sigma-Aldrich) was added to the dried sample, and the mixture was incubated at 30°C for 90 minutes. For silylation, 45  $\mu\text{L}$  of *N*-methyl-*N*-trimethylsilyl-trifluoroacetamide (Fluka, Buchs, Switzerland) was added to the mixture, and the mixture was incubated at 37°C for 30 min. An Agilent 7890B GC system (Agilent Technologies, Santa Clara, CA, USA) coupled with a Pegasus HT-TOF-MS (LECO, St. Joseph, MI, USA) was used to analyze metabolites. Sample aliquots of 0.5  $\mu\text{L}$

were injected into the GC in splitless mode. Metabolites were separated on an RTX-5Sil MS column (30-m length, 0.25-mm inner diameter, and 0.25- $\mu\text{m}$  film thickness; Restek, Bellefonte, PA, USA) with an additional 10-m guard column. The oven temperature was set at 50°C for 1 min, ramped to 330°C at a rate of 20°C/min, and held at 330°C for 5 min. Mass spectra were recorded over a mass range of 85–500  $m/z$  at an acquisition rate of 16 spectra/s. The temperatures of the ion source and transfer line of the TOF-MS were 250°C and 280°C, respectively. The electron ionization energy was 70 eV. Chroma TOF Software C version (LECO) was used for the detection and deconvolution of peaks and mass spectra. BinBase was used for the identification and relative quantification of metabolites from preprocessed data by matching mass spectra and retention indices of peaks with the customized reference mass spectral and retention index libraries, acquired using authentic standards with identical data acquisition parameters for the Fiehn and NIST libraries.<sup>71,72</sup> Peaks with mass spectral similarities above 700, in comparison to their authentic standards in the libraries, were regarded as authentic metabolites. Intensities of metabolites were reported as peak heights of their unique ion intensities. For management of missing values, the lowest background intensity was subtracted from the intensity of the quantified ion in its retention time region  $\pm 5\text{s}$ , using MZmine. Data were then analyzed using the Mann-Whitney U test, performed with STATISTICA (ver. 7.1; StatSoft, Tulsa, OK, USA) and MetaMapp performed using MetaMapp and Cytoscape software packages.<sup>73</sup> The intensity of each metabolite was converted to a z-score and expressed as a heat map using the MultiExperiment Viewer application. Metabolite set enrichment pathway analysis was performed using MetaboAnalyst<sup>74</sup>.

### **Quantification of AzA in fecal samples and liver and adipose tissues of mice**

Concentrations of AzA in liver, fecal, and adipose tissue samples were determined by GC/TOF-MS. An analytical standard of AzA (purity > 98.5%) was purchased from, Sigma-Aldrich and analyzed



using the above GC/TOF–MS protocol. The standard curve for quantification of AzA was made based on the height of the unique mass ( $m/z$ : 129) of AzA ( $R^2 = 1.000$ ). The height of the unique mass of AzA in the GC/TOF–MS data from each liver, fecal, and adipose tissue sample was converted to the absolute concentration using the standard curve.

### **3-(4,5-dimethylthiazol-2-yl)-2,5-diphenyltetrazolium bromide (MTT) assay**

GLUtag cell viability was analyzed using MTT assay as previously described.<sup>5</sup> GLUtag cells were seeded in culture medium for 2 d. The cells were then treated with increasing concentrations of AzA up to 500  $\mu$ M. After 24 h, the culture medium was removed, and 1 ml of culture medium with 10% MTT solution was added and incubated for 3 h. The MTT solution was removed and the cells were dried. Then, 1 ml of dimethyl sulfoxide was added and incubated for 2 h with mild shaking. The absorbance at 570 nm was measured in a Multiskan GO microplate spectrophotometer (Thermo Fisher Scientific, Carlsbad, CA, USA).

### **Statistical analysis**

Data are expressed as the mean  $\pm$  SEM were analyzed using GraphPad Prism 8.0 (GraphPad Software). The significance of differences between the two groups was evaluated by two-tailed unpaired Student's *t* test for samples with normal distribution or the Mann-Whitney U test for samples that were not normally distributed. The significance of differences among three or more groups was evaluated by one-way ANOVA with Bonferroni's multiple comparisons test. Statistical analysis of microbiome and metabolomics results are described in the corresponding sections. In all analyses,  $P < .05$  was considered to indicate statistical significance.

### **Availability of data**

The sequences from this study were deposited in the European Nucleotide Archive under the study accession number ERP119149 (16S rRNA sequencing) and PRJEB38229 (RNA-seq).

### **Disclosure statement**

No potential conflicts of interest were disclosed.

### **Author contributions**

SJL designed the study. CW, MYJ, JYK, GL, JSK, YEC, HK, CHC, JK, MKP, and YKS acquired the data and performed experiments. SJL, GPK, KHK, SHK and GHS advised on the data analysis. CW, MYJ, JYK, GL, and SJL wrote the manuscript. All authors read and approve the manuscript.

### **Funding**

This work was supported by a National Research Foundation of Korea (NRF) grants funded by the Korean government (MSIT) (Grant Nos. NRF-2018R1A4A1022589, NRF-2019R1A2C3005227, and NRF-2019R1I1A1A01064105).

### **ORCID**

Sung-Joon Lee  <http://orcid.org/0000-0001-8683-3377>

### **References**

1. Ache BW, Young JM. Olfaction: diverse species, conserved principles. *Neuron*. 2005;48:417–430. doi:10.1016/j.neuron.2005.10.022.
2. Niimura Y. Olfactory receptor multigene family in vertebrates: from the viewpoint of evolutionary genomics. *Curr Genomics*. 2012;13:103–114. doi:10.2174/138920212799860706.
3. Flegel C, Manteniots S, Osthold S, Hatt H, Gisselmann G. Expression profile of ectopic olfactory receptors determined by deep sequencing. *PLoS One*. 2013;8:e55368. doi:10.1371/journal.pone.0055368.
4. Lee SJ, Depoortere I, Hatt H. Therapeutic potential of ectopic olfactory and taste receptors. *Nat Rev Drug Discov*. 2019;18:116–138.
5. Wu C, Hwang SH, Jia Y, Choi J, Kim YJ, Choi D, et al. Olfactory receptor 544 reduces adiposity by steering fuel preference toward fats. *J Clin Invest*. 2017;127:4118–4123. doi:10.1172/JCI89344.
6. Thack TT, Wu C, Hwang KY, Lee SJ. Azelaic acid induces mitochondrial biogenesis in skeletal muscle by activation of olfactory receptor 544. *Front Physiol*. 2020;11(Article):329. doi:10.3389/fphys.2020.00329.
7. Kang N, Bahk YY, Lee N, Jae Y, Cho YH, Ku CR, et al. Olfactory receptor Olfr544 responding to azelaic acid regulates glucagon secretion in alpha-cells of mouse pancreatic islets. *Biochem Biophys Res Commun*. 2015;460:616–621. doi:10.1016/j.bbrc.2015.03.078.

8. Grego AV, Mingrone G. Dicarboxylic acids, an alternate fuel substrate in parenteral nutrition: an update. *Clin Nutr.* 1995;14:143–148. doi:10.1016/S0261-5614(95)80011-5.
9. Litvinov D, Selvarajan K, Garelnabi M, Brophy L, Parthasarathy S. Anti-atherosclerotic actions of azelaic acid, an end product of linoleic acid peroxidation, in mice. *Atherosclerosis.* 2010;209:449–454. doi:10.1016/j.atherosclerosis.2009.09.076.
10. Muthulakshmi S, Saravanan R. Protective effects of azelaic acid against high-fat diet-induced oxidative stress in liver, kidney and heart of C57BL/6J mice. *Mol Cell Biochem.* 2013;377:23–33. doi:10.1007/s11010-013-1566-1.
11. Bladon PT, Burke BM, Cunliffe WJ, Forster RA, Holland KT, King K. Topical azelaic acid and the treatment of acne: a clinical and laboratory comparison with oral tetracycline. *Br J Dermatol.* 1986;114:493–499. doi:10.1111/j.1365-2133.1986.tb02856.x.
12. Breathnach AS. Azelaic acid: potential as a general anti-tumoural agent. *Med Hypotheses.* 1999;52:221–226.
13. Mastrofrancesco A, Ottaviani M, Aspate N, Cardinali G, Izzo E, Graupe K, et al. Azelaic acid modulates the inflammatory response in normal human keratinocytes through PPAR $\gamma$  activation. *Exp Dermatol.* 2010;19:813–820. doi:10.1111/j.1600-0625.2010.01107.x.
14. Murphy KG, Dhillo WS, Bloom SR. Gut peptides in the regulation of food intake and energy homeostasis. *Endocr Rev.* 2006;27:719–727. doi:10.1210/er.2006-0028.
15. Leech CA, Dzhura I, Chepurny OG, Kang G, Schwede F, Genieser HG, et al. Molecular physiology of glucagon-like peptide-1 insulin secretagogue action in pancreatic beta cells. *Prog Biophys Mol Biol.* 2011;107:236–247. doi:10.1016/j.pbiomolbio.2011.07.005.
16. Lim GE, Brubaker PL. Glucagon-like peptide 1 secretion by the L-cell - The view from within. *Diabetes.* 2006;55:S70–S7. doi:10.2337/db06-S020.
17. Van De Guchte M, Blottiere HM, Dore J. Humans as holobionts: implications for prevention and therapy. *Microbiome.* 2018;6:81. doi:10.1186/s40168-018-0466-8.
18. Yang JY, Lee YS, Kim Y, Lee SH, Ryu S, Fukuda S, et al. Gut commensal *Bacteroides acidifaciens* prevents obesity and improves insulin sensitivity in mice. *Mucosal Immunol.* 2017;10:104–116. doi:10.1038/mi.2016.42.
19. Yue S, Zhao D, Peng C, Tan C, Wang Q, Gong J. Effects of theabrownin on serum metabolites and gut microbiome in rats with a high-sugar diet. *Food Funct.* 2019;10:7063–7080. doi:10.1039/C9FO01334B.
20. Wang H, Zhang X, Wang S, Li H, Lu Z, Shi J, et al. Mannan-oligosaccharide modulates the obesity and gut microbiota in high-fat diet-fed mice. *Food Funct.* 2018;9:3916–3929. doi:10.1039/C8FO00209F.
21. Douglas GM, Maffei VJ, Zaneveld J, Yurgel SN, Brown JR, Taylor CM, et al. PICRUSt2: an improved and extensible approach for metagenome inference. *BioRxiv.* 2019;672295. doi:10.1101/672295
22. Jackson AA, Persaud C, Hall M, Smith S, Evans N, Rutter N. Urinary excretion of 5-L-oxoproline (pyroglutamic acid) during early life in term and preterm infants. *Arch Dis Child Fetal Neonatal Ed.* 1997;76:F152–7. doi:10.1136/fn.76.3.F152.
23. Ogasawara Y, Funakoshi M, Ishii K. Determination of reduced nicotinamide adenine dinucleotide phosphate concentration using high-performance liquid chromatography with fluorescence detection: ratio of the reduced form as a biomarker of oxidative stress. *Biol Pharm Bull.* 2009;32:1819–1823. doi:10.1248/bpb.32.1819.
24. Van Dijck P, Colavizza D, Smet P, Thevelein JM. Differential importance of trehalose in stress resistance in fermenting and nonfermenting *Saccharomyces cerevisiae* cells. *Appl Environ Microbiol.* 1995;61:109–115. doi:10.1128/aem.61.1.109-115.1995.
25. Karagiannides I, Pothoulakis C. Obesity, innate immunity and gut inflammation. *Curr Opin Gastroenterol.* 2007;23:661–666. doi:10.1097/MOG.0b013e3282c8c8d3.
26. Belkaid Y, Harrison OJ. Homeostatic immunity and the microbiota. *Immunity.* 2017;46:562–576. doi:10.1016/j.immuni.2017.04.008.
27. Cani PD. Human gut microbiome: hopes, threats and promises. *Gut.* 2018;67:1716–1725. doi:10.1136/gutjnl-2018-316723.
28. Eissele R, Goke R, Willemer S, Harthus HP, Vermeer H, Arnold R, et al. Glucagon-like peptide-1 cells in the gastrointestinal tract and pancreas of rat, pig and man. *Eur J Clin Invest.* 1992;22:283–291. doi:10.1111/j.1365-2362.1992.tb01464.x.
29. Campbell JE, Drucker DJ. Pharmacology, physiology, and mechanisms of incretin hormone action. *Cell Metab.* 2013;17:819–837. doi:10.1016/j.cmet.2013.04.008.
30. Manigault KR, Thurston MM. Liraglutide: a glucagon-like peptide-1 agonist for chronic weight management. *Consult Pharm.* 2016;31:685–697. doi:10.4140/TCP.n.2016.685.
31. Khera R, Murad MH, Chandar AK, Dulai PS, Wang Z, Prokop LJ, et al. Association of pharmacological treatments for obesity with weight loss and adverse events: a systematic review and meta-analysis. *JAMA.* 2016;315:2424–2434. doi:10.1001/jama.2016.7602.
32. Reimann F, Gribble FM. Glucose-sensing in glucagon-like peptide-1-secreting cells. *Diabetes.* 2002;51:2757–2763. doi:10.2337/diabetes.51.9.2757.
33. Roder PV, Geillinger KE, Zietek TS, Thorens B, Koepsell H, Daniel H, The role of SGLT1 and GLUT2 in intestinal glucose transport and sensing. *PLoS One.* 2014;9:e89977. doi:10.1371/journal.pone.0089977.

34. Tolhurst G, Heffron H, Lam YS, Parker HE, Habib AM, Diakogiannaki E, et al. Short-chain fatty acids stimulate glucagon-like peptide-1 secretion via the G-protein-coupled receptor FFAR2. *Diabetes*. 2012;61:364–371. doi:10.2337/db11-1019.
35. Oya M, Kitaguchi T, Pais R, Reimann F, Gribble F, Tsuboi T. The G protein-coupled receptor family C group 6 subtype A (GPRC6A) receptor is involved in amino acid-induced glucagon-like peptide-1 secretion from GLUTag cells. *J Biol Chem*. 2013;288:4513–4521. doi:10.1074/jbc.M112.402677.
36. Harada K, Kitaguchi T, Kamiya T, Aung KH, Nakamura K, Ohta K, et al. Lysophosphatidylinositol-induced activation of the cation channel TRPV2 triggers glucagon-like peptide-1 secretion in enteroendocrine L cells. *J Biol Chem*. 2017;292:10855–10864. doi:10.1074/jbc.M117.788653.
37. Harada K, Sakaguchi H, Sada S, Ishida R, Hayasaka Y, Tsuboi T. Bitter tastant quinine modulates glucagon-like peptide-1 exocytosis from clonal GLUTag enteroendocrine L cells via actin reorganization. *Biochem Biophys Res Commun*. 2018;500:723–730. doi:10.1016/j.bbrc.2018.04.143.
38. Lee JH, Wen X, Cho H, Koo SH. CREB/CRTC2 controls GLP-1-dependent regulation of glucose homeostasis. *FASEB J*. 2018;32:1566–1578. doi:10.1096/fj.201700845R.
39. Harada K, Kitaguchi T, Tsuboi T. Integrative function of Adrenaline receptors for glucagon-like peptide-1 exocytosis in enteroendocrine L cell line GLUTag. *Biochem Biophys Res Commun*. 2015;460:1053–1058. doi:10.1016/j.bbrc.2015.03.151.
40. Vollert S, Kaessner N, Heuser A, Hanauer G, Dieckmann A, Knaack D, et al. The glucose-lowering effects of the PDE4 inhibitors roflumilast and roflumilast-N-oxide in *db/db* mice. *Diabetologia*. 2012;55:2779–2788. doi:10.1007/s00125-012-2632-z.
41. Miyamoto Y, Itoh K. *Bacteroides acidifaciens* sp. nov., isolated from the caecum of mice. *Int J Syst Evol Microbiol*. 2000;50(Pt 1):145–148. doi:10.1099/00207713-50-1-145.
42. Zhang Q, Xiao X, Zheng J, Li M, Yu M, Ping F, et al. Influence of maternal inulin-type prebiotic intervention on glucose metabolism and gut microbiota in the offspring of C57BL mice. *Front Endocrinol (Lausanne)*. 2019;10:675. doi:10.3389/fendo.2019.00675.
43. Canfora EE, Meex RCR, Venema K, Blaak EE. Gut microbial metabolites in obesity, NAFLD and T2DM. *Nat Rev Endocrinol*. 2019;15:261–273. doi:10.1038/s41574-019-0156-z.
44. Fernandez-Veledo S, Ceperuelo-Mallafre V, Vendrell J. Rethinking succinate: an unexpected hormone-like metabolite in energy homeostasis. *Trends Endocrinol Metab*. 2021;32:680–692. doi:10.1016/j.tem.2021.06.003.
45. De Vadder F, Kovatcheva-Datchary P, Zitoun C, Duchamp A, Backhed F, Mithieux G. Microbiota-produced succinate improves glucose homeostasis via intestinal gluconeogenesis. *Cell Metab*. 2016;24:151–157. doi:10.1016/j.cmet.2016.06.013.
46. Liu Y, Heath AL, Galland B, Rehrer N, Drummond L, Wu XY, et al. Substrate use prioritization by a coculture of five species of gut bacteria fed mixtures of arabinoxylan, xyloglucan, beta-glucan, and pectin. *Appl Environ Microbiol*. 2020;86:e01905-19. doi:10.1128/AEM.01905-19.
47. Wan Y, Yuan J, Li J, Li H, Yin K, Wang F, et al. Overweight and underweight status are linked to specific gut microbiota and intestinal tricarboxylic acid cycle intermediates. *Clin Nutr*. 2020;39:3189–3198. doi:10.1016/j.clnu.2020.02.014.
48. Arai C, Kohguchi M, Akamatsu S, Arai N, Yoshizane C, Hasegawa N, et al. Trehalose suppresses lipopolysaccharide-induced osteoclastogenesis bone marrow in mice. *Nutr Res*. 2001;21:993–999. doi:10.1016/S0271-5317(01)00315-3.
49. Yoshizane C, Arai N, Arai C, Yamamoto M, Nishizaki Y, Hanaya T, et al. Trehalose suppresses osteoclast differentiation in ovariectomized mice: correlation with decreased in vitro interleukin-6 production by bone marrow cells. *Nutr Res*. 2000;20:1485–1491. doi:10.1016/S0271-5317(00)80029-9.
50. Arai C, Miyake M, Matsumoto Y, Mizote A, Yoshizane C, Hanaya Y, et al. Trehalose prevents adipocyte hypertrophy and mitigates insulin resistance in mice with established obesity. *J Nutr Sci Vitaminol (Tokyo)*. 2013;59:393–401. doi:10.3177/jnsv.59.393.
51. Arai C, Arai N, Arai S, Yoshizane C, Miyata S, Mizote A, et al. Continuous intake of trehalose induces white adipose tissue browning and enhances energy metabolism. *Nutr Metab (Lond)*. 2019;16:45. doi:10.1186/s12986-019-0373-4.
52. Kobayashi M, Yasukawa H, Arikawa T, Deguchi Y, Mizushima N, Sakurai M, et al. Trehalose induces SQSTM1/p62 expression and enhances lysosomal activity and antioxidative capacity in adipocytes. *FEBS Open Bio*. 2021;11:185–194. doi:10.1002/2211-5463.13055.
53. Higgins CB, Zhang Y, Mayer AL, Fujiwara H, Stothard AI, Graham MJ, et al. Hepatocyte ALOXE3 is induced during adaptive fasting and enhances insulin sensitivity by activating hepatic PPAR $\gamma$ . *JCI Insight*. 2018;3:e120794. doi:10.1172/jci.insight.120794.
54. Lee YS, Jun HS. Anti-Inflammatory Effects of GLP-1-based therapies beyond glucose control. *Mediators Inflamm*. 2016;2016:3094642. doi:10.1155/2016/3094642.
55. Yusta B, Baggio LL, Koehler J, Holland D, Cao X, Pinnell LJ, et al. GLP-1R agonists modulate enteric immune responses through the intestinal intraepithelial lymphocyte GLP-1R. *Diabetes*. 2015;64:2537–2549. doi:10.2337/db14-1577.

56. Miura Y. The biological significance of omega-oxidation of fatty acids. *Proc Jpn Acad Ser B Phys Biol Sci*. 2013;89:370–382. doi:10.2183/pjab.89.370.
57. Gallagher RS, Ananth R, Granger K, Bradley B, Anderson JV, Fuerst EP. Phenolic and short-chained aliphatic organic acid constituents of wild oat (*Avena fatua* L.) seeds. *J Agric Food Chem*. 2010;58:218–225. doi:10.1021/jf9038106.
58. Thellin O, Zorzi W, Lakaye B, De Borman B, Coumans B, Hennen G, et al. Housekeeping genes as internal standards: use and limits. *J Biotechnol*. 1999;75:291–295. doi:10.1016/S0168-1656(99)00163-7.
59. Harach T, Pols TW, Nomura M, Maida A, Watanabe M, Auwerx J, et al. TGR5 potentiates GLP-1 secretion in response to anionic exchange resins. *Sci Rep*. 2012;2:430. doi:10.1038/srep00430.
60. Karstoft K, Winding K, Knudsen SH, James NG, Scheel MM, Olesen J, et al. Mechanisms behind the superior effects of interval vs continuous training on glycaemic control in individuals with type 2 diabetes: a randomised controlled trial. *Diabetologia*. 2014;57:2081–2093. doi:10.1007/s00125-014-3334-5.
61. Pichette J, Fynn-Sackey N, Gagnon J. Hydrogen sulfide and sulfate prebiotic stimulates the secretion of GLP-1 and improves glycemia in male mice. *Endocrinology*. 2017;158:3416–3425. doi:10.1210/en.2017-00391.
62. Cani PD, Bibiloni R, Knauf C, Waget A, Neyrinck AM, Delzenne NM, et al. Changes in gut microbiota control metabolic endotoxemia-induced inflammation in high-fat diet-induced obesity and diabetes in mice. *Diabetes*. 2008;57:1470–1481. doi:10.2337/db07-1403.
63. Boue S, Fortgang I, Levy RJ Jr., Bhatnagar D, Burow M, Fahey G, et al. A novel gastrointestinal microbiome modulator from soy pods reduces absorption of dietary fat in mice. *Obesity (Silver Spring)*. 2016;24:87–95. doi:10.1002/oby.21197.
64. Bahar B, O'Doherty JV, Vigors S, Sweeney T. Activation of inflammatory immune gene cascades by lipopolysaccharide (LPS) in the porcine colonic tissue *ex-vivo* model. *Clin Exp Immunol*. 2016;186:266–276. doi:10.1111/cei.12839.
65. Bolyen E, Rideout JR, Dillon MR, Bokulich NA, Abnet CC, Al-Ghalith GA, et al. Reproducible, interactive, scalable and extensible microbiome data science using QIIME 2. *Nat Biotechnol*. 2019;37:852–857.
66. Callahan BJ, McMurdie PJ, Rosen MJ, Han AW, Johnson AJA, Holmes SP. DADA2: high-resolution sample inference from Illumina amplicon data. *Nat Methods*. 2016;13:581. doi:10.1038/nmeth.3869.
67. McDonald D, Price MN, Goodrich J, Nawrocki EP, DeSantis TZ, Probst A, et al. An improved Greengenes taxonomy with explicit ranks for ecological and evolutionary analyses of bacteria and archaea. *ISME J*. 2012;6:610. doi:10.1038/ismej.2011.139.
68. Oksanen J, Kindt R, Legendre P, O'Hara B, Stevens MHH, Oksanen MJ, et al. The vegan package. *Community Ecology Package*. 2007;10:719.
69. Liaw A, Wiener M. Classification and regression by randomForest. *R News*. 2002;2:18–22.
70. Turrone S, Fiori J, Rampelli S, Schnorr SL, Consolandi C, Barone M, et al. Fecal metabolome of the Hadza hunter-gatherers: a host-microbiome integrative view. *Sci Rep*. 2016;6:32826. doi:10.1038/srep32826.
71. Kind T, Wohlgemuth G, Lee DY, Lu Y, Palazoglu M, Shahbaz S, et al. FiehnLib: mass spectral and retention index libraries for metabolomics based on quadrupole and time-of-flight gas chromatography/mass spectrometry. *Anal Chem*. 2009;81:10038–10048. doi:10.1021/ac9019522.
72. Skogerson K, Wohlgemuth G, Barupal DK, Fiehn O. The volatile compound BinBase mass spectral database. *BMC Bioinform*. 2011;12:321. doi:10.1186/1471-2105-12-321.
73. Barupal DK, Haldiya PK, Wohlgemuth G, Kind T, Kothari SL, Pinkerton KE, et al. MetaMapp: mapping and visualizing metabolomic data by integrating information from biochemical pathways and chemical and mass spectral similarity. *BMC Bioinform*. 2012;13:99. doi:10.1186/1471-2105-13-99.
74. Pang Z, Chong J, Zhou G, de Lima Morais DA, Chang L, Barrette M, et al. MetaboAnalyst 5.0: narrowing the gap between raw spectra and functional insights. *Nucleic Acids Res*. 2021;49:W388–W96. doi:10.1093/nar/gkab382.